FEDSM2021-65393

CFD ANALYSIS AND WIND TUNNEL TESTING OF HUMAN POWERED VEHICLE DRAG COEFFICIENTS

Tony Estrada, Kevin R. Anderson, Ivan Gundersen, Chuck Johnston
California State Polytechnic University
Pomona, CA

ABSTRACT

This paper presents results of Computational Fluid Dynamics (CFD) modeling and experimental wind tunnel testing to predict the drag coefficient for a Human Powered Vehicle (HPV) entered in the World Human Powered Speed Challenge (WHPSC). Herein, a comparison of CFD to wind tunnel test data is presented for ten different HPV designs. The current study reveals that streamlining the nose cone, tail cone, and wheel housing allows for a reduction of drag forces in critical areas, and a reduced drag coefficient. This allows for a selection to be made during the design phase, prior to manufacturing. Drag coefficients were found to be in the range of $0.133 < C_D < 0.273$, depending on the type of HPV considered. Wind tunnel testing was performed on scale models of the HPV showing agreement to the CFD results on average to within 16%. The wind tunnel testing showed a 7.7% decrease in drag coefficient from the baseline HPV of 2019 to the baseline HPV of 2020. Thus, the wind tunnel data supported by CFD analysis was used to assist in the design of the HPV.

Keywords: Human Powered Vehicle, CFD, Wind Tunnel

NOMENCLATURE

A	frontal area
C_D	drag coefficient
F_D	drag force
V	air velocity
ρ	air density
CFD	Computational Fluid Dynamics
HPV	Human Powered Vehicle

1. INTRODUCTION

The World Human Powered Speed Challenge (WHPSC) is a competition where cyclists race to break the human powered land speed record, 89.59 mph. The WHPSC is held in Battle Mountain, Nevada, which has a section of road specifically prepared for human-powered vehicle (HPV) racing by the Nevada Department of Transportation. The Sprocket Rocket, a 5-person quad cycle, is one of the Human Powered Vehicles competing in the WHPSC. In 2019 the Sprocket Rocket achieved a top speed of 56.4 mph, making it the second fastest human powered vehicle with 3 or more riders. In 2021 they will attempt to reach a speed of 63 mph, by modifying their design, to break a world record. Figure 1 shows the Sprocket Rocket human powered vehicle studied in this paper.

FIGURE 1: SPROCKET ROCKET HUMAN POWERED VEHICLE

Reducing the drag force on The Sprocket Rocket would potentially allow the power generated by the cyclists to increase velocity instead of overcoming the drag force. This can be done

by streamlining, altering the geometry of the vehicle to reduce the Drag Coefficient, C_D. A reduction of drag coefficients in the design phase using Computational Fluid Dynamics (CFD) software, and a scaled Wind Tunnel test allows for optimization of flow conditions on the vehicle. Drag is the resulting force caused by the resistance of the fluid opposite to the direction of motion. The drag coefficient [1,2,3] is given by Eqn. (1)

$$C_D = \frac{F_D}{\frac{1}{2}\rho V^2 A} \qquad (1)$$

where C_D is the coefficient of drag, F_D is the Drag Force, ρ is the density of the surrounding fluid, V is the velocity of the fluid, and A is the frontal area. The actual drag force is composed of friction drag (aka skin friction) and pressure drag (aka form drag).

$$C_D = C_{D,press} + C_{D,fric} \qquad (2)$$

where $C_{D,press}$ is the coefficient of pressure drag and $C_{D,fric}$ is the coefficient of friction drag. The friction drag is caused by the shear stress of the moving fluid over a surface, while the pressure drag is caused by a pressure gradient in the flow. This pressure gradient is caused by the separation of the boundary layer from the body, which occurs at the separation point. This separation point is followed by the wake region, a low-pressure region. For smooth surface streamlined HPVs such as the one considered herein, the form drag is small and the friction drag is large. Typically the total drag is composed of 10% of form drag and 90% of friction drag [1,2,3].

2. LITERATURE REVIEW

This section of the paper presents a review of recent related studies to the present work. In the study of [4] aerodynamic performance of HPVs are discussed followed by a case study using CFD models to address laminar-turbulent transition of the boundary layer on the HPV. In the study of [5] fairing design is aided using CFD. In the research study of [6], CFD and wind tunnel investigation of a human powered vehicle (HPV) are presented to analyze the HPV's drag efficiency in a high profile HPV speed record competition. In the study of [7], the student design team examine the aerodynamic behavior of two production HPVs using both on road tests and CFD modelling. The study of [8] presents CFD work for a single driver HPV which was entered at the WHPSC in 2015.

3. MATERIALS AND METHODS

Here we discuss the methodology used by the CFD calculations followed by the description of the wind tunnel testing.

2.1 CFD Methodology

For the CFD computations ANSYS FLUENT was used. The Navier Stokes equations and the k-ε turbulence model governing equations solved are as follows

$$\frac{\partial \rho}{\partial t} + \frac{\partial v}{\partial x_k}(\rho u_k) = 0 \qquad (3)$$

$$\rho\left(\frac{Du_i}{Dt}\right) = -\frac{\partial p}{\partial x_i} + \mu \nabla^2 u_i + \rho f_{b,i} \qquad (4)$$

$$\frac{Dk}{Dt} = \frac{\partial}{\partial x_j}\left(\frac{v_t}{\sigma_k}\frac{\partial k}{\partial x_j}\right) + v_t \frac{\partial \overline{u_i}}{\partial x_j}\left(\frac{\partial \overline{u_i}}{\partial x_j} + \frac{\partial \overline{u_j}}{\partial x_i}\right) - \varepsilon \qquad (5)$$

$$\frac{D\varepsilon}{Dt} = \frac{\partial}{\partial x_j}\left(\frac{v_t}{\sigma_\varepsilon}\frac{\partial \varepsilon}{\partial x_j}\right) + C_1 v_t \frac{\varepsilon}{k}\frac{\partial \overline{u_i}}{\partial x_j}\left(\frac{\partial \overline{u_i}}{\partial x_j} + \frac{\partial \overline{u_j}}{\partial x_i}\right) - \frac{C_2\varepsilon^2}{k} \qquad (6)$$

The standard k-ε wall functions were used for the turbulence modeling. A PC with an 8-core/16 thread CPU processor running at 4.1 GHz, 48 GB of RAM at 3066 MHz and an Nvidia RTX 2080 GPU was used to carry out the simulations.

As shown in Figure 2, ten different configuration of the HPV were simulation using the CFD model.

Model	Geometry of HPV
1	2019
2	2019 CONES REVERSED
3	2019 TWO TAIL CONES
4	2020
5	2020 WITH 2019 TAIL
6	2020 MONOPANT
7	2020 JETSKI
8	2020 JETSKI TALL TAIL
9	2020 MONO LONG 2019 TAIL
10	AEROVELO ETA HPV

FIGURE 2: HPV MODELS STUDIED

The various configurations of Figure 2 were realized by interchanging the nose cones, tail cones and wheel housing of the HPV. The following models were tested using three different environments in order to simulate road effects for the Sprocket Rocket HPV. The three environments simulated using CFD were as follows i) in air, ii) in proximity to a stationary road and iii) in the vicinity of a moving road. As shown in Figure 3, the CFD model was built by making creating and enclosure encompassing the HPV CAD model. Figure 3 shows the boundary conditions of a velocity inlet, zero pressure exit, and road (moving or stationary), the HPV and the enclosure, respectively. The enclosure surrounding the HPV was created using a non-uniform Cushion and had the following dimensions: +/- 12.5 feet in the X and Y directions, and +/- 22.5 feet in the Z direction, parallel to the flow. The enclosure for both the moving and stationary Road cases were as follows: +/- 12.5 feet in the X direction, + 12.5 ft/-.1667 ft in the Y direction, and +/- 22.5 ft in the Z direction. A Boolean CAD operation was utilized to subtract the CAD model from the enclosure and create the fluid zone which was then meshed. Each CFD model was initially meshed using FLUENT's default mesh function. The mesh was then refined using mesh refinements.
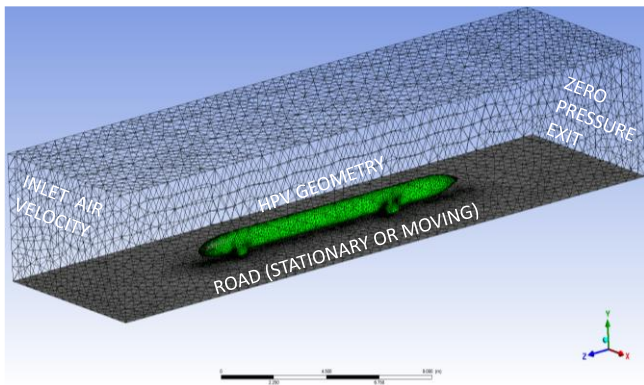

FIGURE 3: CFD MODEL SET UP

The ANSYS / FLUENT boundary conditions were prescribed using as follows: the face in front of the model was named a "Velocity Inlet", while the face behind the model was named a "Pressure Outlet". The remaining faces in the Air and Stationary Road cases, were named "Wall". In the moving road cases, the face below the HPV model was named "Moving Wall", while the remaining faces remained "Wall". The moving wall was assigned a velocity to mimic the motion of the road moving relative to the HPV. The boundary conditions illustrated in Figure 3 are summarized in Table 1.

TABLE 1: CFD MODEL BOUNDARY CONDITIONS

INLET VELOCITY MAGNITUDE	24.59 m/s
OUTLET PRESSURE	0 Pa
WALL SURFACE ROUGHNESS	0.003175 m
WALL VELOCITY (MOVING ROAD)	24.59 m/s

The freestream Reynolds number based upon the input velocity in the CFD model corresponds to $Re = 1.92 \times 10^7$ based upon the overall length scale of the HPV. The pertinent CFD solver settings used were for pressure-velocity coupling, SIMPLE Scheme-Coupled for the pressure velocity coupling, Green-Gauss Node Based for the gradient discretization, and Second Order equations were used for both Pressure and momentum equations.

2.2 Mesh Independence Study

A mesh independence study was completed to verify the results using the allowable number of elements in ANSYS FLUENT. This study was completed using the Model 4 of Figure 2, the 2020 model with a moving road. Figure 4 shows the results of the mesh independence study. The number of elements were increased, and the simulation repeated until 512,000 elements were reached. The drag coefficient was $C_D = 0.21608$, for 512K elements, and $C_D = 0.21884$ for 419K elements. The mesh for the other simulations was set to 419K elements.
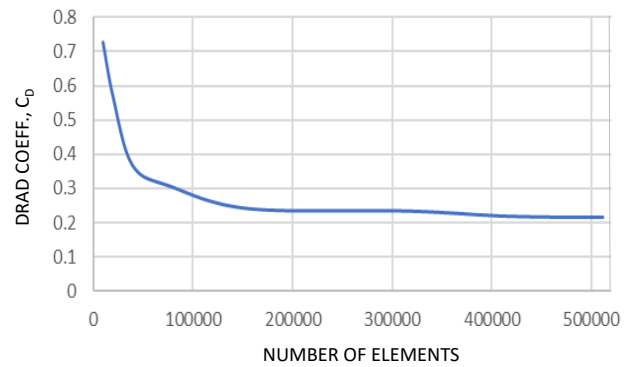

FIGURE 4: MESH INDEPENDENCE STUDY

2.3 Road Roughness Coefficient Study

In order to assess the sensitivity of the roughness coefficient of the wall used to model the road, a numerical study carried out using Model 4 of Figure 2 the 2020 model with a moving road. The results of the road surface roughness coefficient study are shown in Figure 5. As seen in Figure 5, the value for the drag coefficient C_D varies between roughness constants as the roughness height parameter is increased. The CFD simulations were completed with a roughness constant of unity, and a roughness height of 1/8 inch to mimic the surface conditions of the road.
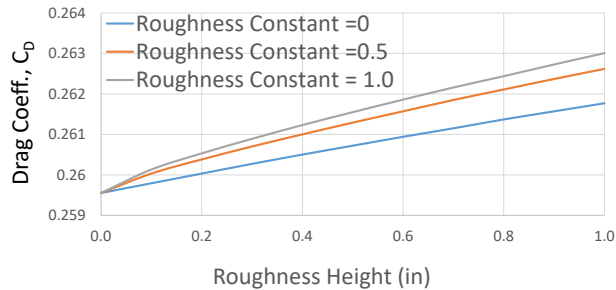
FIGURE 5: SURFACE ROUGHNESS SENSITIVITY STUDY

2.4 Aerovelo ETA Bike CFD Model

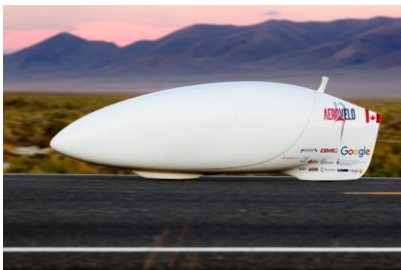The Aerovelo ETA HPV (Model 10 of Figure 2) is shown in Figure 6.

FIGURE 6: AEROVELO ETA HPV [9]

Herein, the Aerovelo ETA HPV is used as a reference value, i.e. we compare our HPV drag coefficients to the Aerovelo ETA single person HPV drag coefficient for the purpose of sanity checking our results, since we do not expect our HPV drag coefficients to be any lower than that of the Aerovelo ETA HPV. In order to illustrate the simulation process we present the CFD simulation set up and results for the Aerovelo ETA HPV in Figure 7 and Figure 8. The CFD simulation of Figure 8 is for a no road simulation, which gives $C_D = 0.135$.
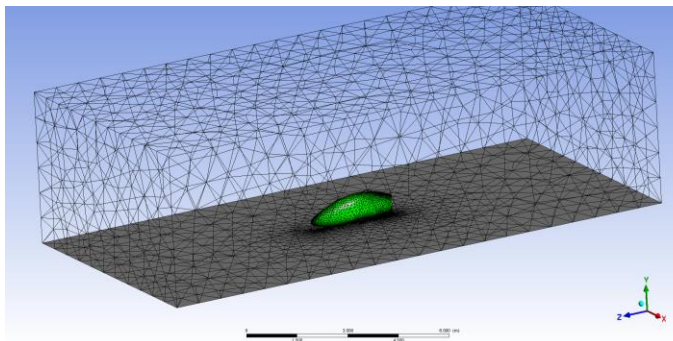

FIGURE 7: CFD MODEL FOR AEROVELO ETA HPV

The drag coefficient convergence history versus the number of iterations for the Aerovelo ETA HPV is shown in Figure 8.
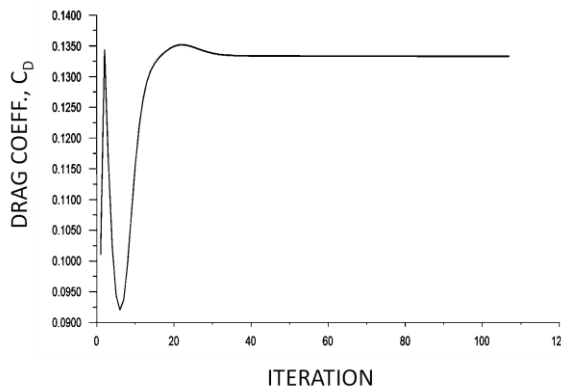

FIGURE 8: DRAG COEFFICIENT CONVERGENCE FOR AEROVELO ETA HPV

2.5 CFD Model Results

In this section of the paper we present typical velocity and pressure flow field contours of the HPV obtained from the CFD modeling effort. Figure 9 shows pressure contours in the neighborhood leading nose section of the 2020 model (configuration 4 of Figure 2). Figure 10 shows turbulent kinetic energy contours in the vicinity of the leading nose section of the 2020 model (configuration 4 of Figure 2). Figure 11 shows velocity streamlines around the HPV obtained from the CFD analysis.
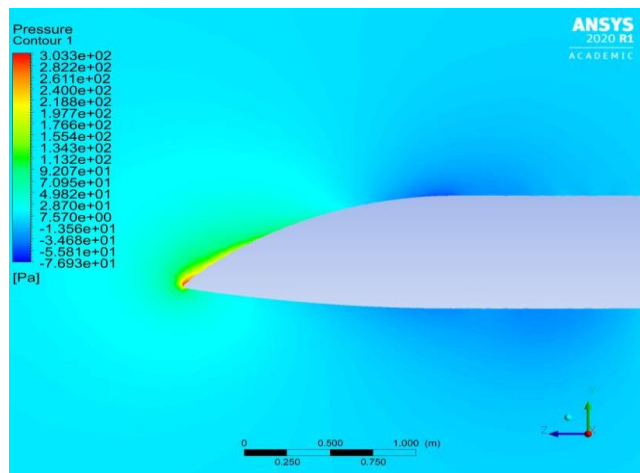

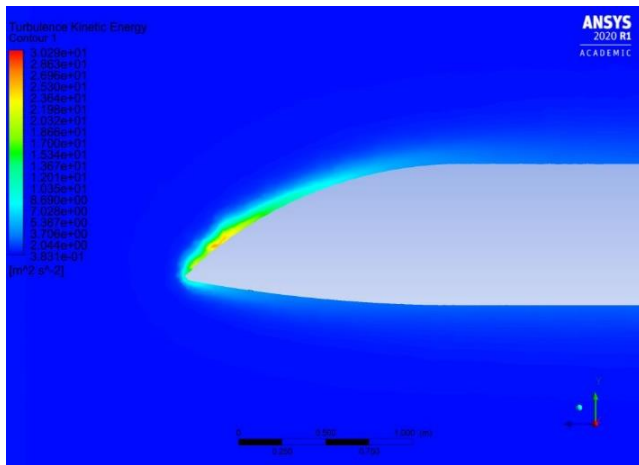**FIGURE 9:** PRESSURE CONTOURS OF MODEL 2020

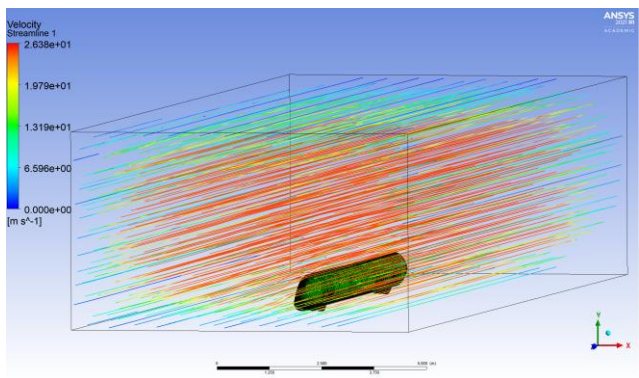**FIGURE 10:** TURBULENT KINETIC ENERGY CONTOURS OF MODEL 2020

FIGURE 11: STREAMLINES AROUND HPV

2.6 Wind Tunnel Experimental Apparatus

In this section of the paper we describe the wind tunnel experimental apparatus. Figure 12 shows the wind tunnel test apparatus.

FIGURE 12: WIND TUNNEL APPARATUS

The test section of the wind tunnel is 96 inches long by 12 inches wide by 12 inches high, with a hanging test specimen and an elevated surface to simulate the road. The wind tunnel has an inlet of 36 inch by 36 inch of honeycomb to straighten the air flow, a 4 inch gap, a screen, and a 12 inch by 12 inch funnel. Air is supplied via ducting to a 10 HP centrifugal fan. The air flow was approximately 25 m/s. Reynolds numbers for the flow were on the order of Re = 1.03×10^5, based on the model dimensions. Due to the extra complexity and cost there was not a moving road in the wind tunnel The wind tunnel tests were carried out with the models hanging in the air, just above a stationary surface to simulate the road. Figure 13 shows a test article mounted in the test section of the wind tunnel.
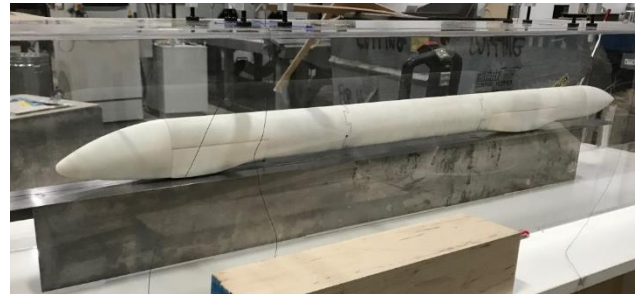

FIGURE 13: TEST ARTICLE MOUNTED IN TEST SECTION OF WIND TUNNEL

Figure 14 shows the various test articles used to measure the ten configurations listed in Figure 2. The test articles were made using 3D printing.

FIGURE 14: WIND TUNNEL TEST ARTICLES

The air flow in the wind tunnel was measured with a TESTO 405i smart probe hot wire anemometer (HWA), along with the temperature, air pressure and humidity. A monofilament line attached to the test specimen to a weight on a digital scale was used to measure the drag force in tenths of grams. The CAD solid models used in the CFD analysis were full scale and the models used in the wind tunnel are 1/12th scale. The full scale vehicle is roughly 45 feet long and the wind tunnel models were 45 inches long by 2 inches wide by 3 inches high. This gave a frontal area about 6% of the wind tunnel cross sectional area.

2 RESULTS AND DISCUSSION

3.1 Comparison of Experimental and CFD Drag Coefficients

The experimental wind tunnel data for the drag coefficients is compared to the CFD determined drag coefficients in Table 2. As seen from Table 2 the CFD drag coefficient data varies from $0.133 < C_D < 0.273$ for the Aerovelo ETA, and the 2019 with

Copyright © 2021 by ASME

fixed road models, respectively. Unfortunately, we did not have a 2019 two tail cone model (Model 3 of Figure 2) or a 2019 cones reversed model (Model 2 of Figure 2) to test in the wind tunnel. For the models shown in Table 2, the agreement between the CFD to the experimental findings was on average within 16%.

TABLE 2: EXPERIMENTAL AND CFD DRAG COEFFICIENT COMPARISON
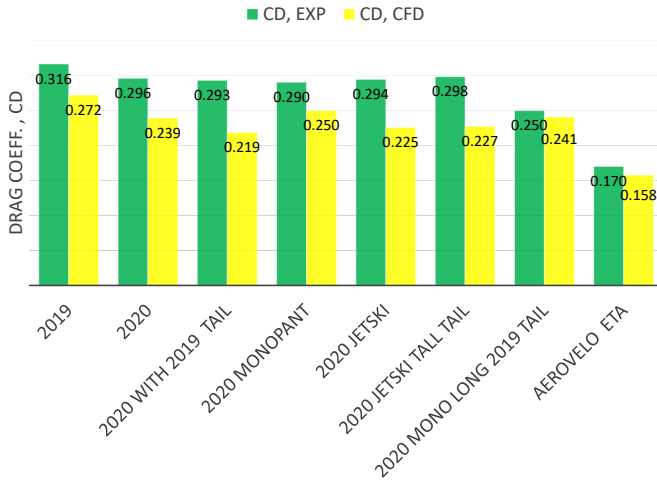
From Table 2 it is seen that the experimental results predict a larger value of the drag coefficient with respect to the CFD simulated drag coefficient for each model considered. The average difference of 16 % between wind tunnel test data and the CFD simulation data is thought to be attributable to two factors. First, variations in the wind tunnel data measurements due to vibrations of the wind tunnel apparatus, and the relatively low forces being recorded by the load scale are thought to have potentially introduced experimental error into the testing results, thus causing the wind tunnel data to overestimate the drag coefficient. Second, the CFD models did not account for the wheels, wheel cut outs, and seams which were present in the 3D printed wind tunnel test articles. Thus, the CFD results may be lower values than they should be in that they do not account for these miscellaneous hardware features.

Nevertheless, the qualitative agreement between the simulation and experimental findings found herein is suffice to support the design stage of the HPV project. The exact agreement of the CFD and the wind tunnel data was not the primary objective of this study. Rather, this study was carried out to illustrate how pragmatic engineering design can be achieved using CFD in concert with wind tunnel testing.

As seen from Table 2, the wind tunnel results agree qualitatively with the CFD results. Namely, the 2020 model (Model 4 of Figure 2) yielded a lower drag coefficient than the 2019 model (Model 1 of Figure 2). The wind tunnel testing showed a 7.7% decrease in drag coefficient from the 2019 (Model 1 of Figure 2) to the 2020 (Model 4 of Figure 2) designs. Table 1 documents the percentage agreement of the drag coefficients obtained from the wind tunnel testing as compared to the CFD simulations.

The 2019 (Model 1 of Figure 2) and 2020 (Model 4 of Figure 2) models were initially tested in the air configuration (without a road surface in close proximity to the wind tunnel model) to see if the 2020 model made any significant improvements on the 2019 model. Eight more models were tested in the Stationary Road configuration. This allowed the bottom wall of the enclosure to act as a road, and have surface roughness properties to applied to it.

Five models were simulated using CFD in the moving road configuration. The bottom wall that was previously stationary was treated as a moving wall boundary condition in the CFD simulations. This allowed for a velocity to be applied to the road, mimicking the road below the human powered vehicle as it moved. The 2020 model produced the best results with a C_D of 0.21608 for the Moving Road configuration, except for the Aerovelo ETA HPV, which is a single rider vehicle which is the fastest human-powered vehicle on earth at 89.59 MPH. Again, we note here that the Aerovelo ETA HPV was tested and simulated herein for reference.

3   CONCLUSION

In this paper we have presented the use of CFD simulations and wind tunnel testing to predict the drag coefficients of a human powered vehicle. The CFD software ANSYS FLUENT was utilized to calculate the Drag Coefficients for ten different models with both a fixed and a moving road configuration. The 2020 model had the lowest drag coefficient value in the moving road configuration with C_D = 0.21608. This is a significant improvement on the 2019 model, which had a C_D = 0.26085 for the moving road configuration. The wind tunnel testing showed a 7.7% decrease in drag coefficient from the 2019 (Model 1 of Figure 2) to the 2020 (Model 4 of Figure 2) designs. Thus, altering the Sprocket Rocket HPV from the 2019 to the 2020 model will lower the drag force on the vehicle while racing, and feasibly increase velocity. Future work will encompass using a finer CFD mesh and enhanced wall treatment option and using the realizable k-ε turbulence model with scalable wall functions (and/or a transitional flow model) in order to resolve the flow field near the wall in an effort to better match our CFD drag coefficient predictions to those of the experimental data. Additionally more wind tunnel testing at higher speeds is planned as future work.

ACKNOWLEDGEMENTS

REFERENCES

[1] Frank M. White, 2011, Fluids Book, Fluid Mechanics, Seventh Edition, McGraw Hill

[2] Sighard F. Hoerner, 1965, Fluid-Dynamic Drag: Practical Information on Aerodynamic Drag and Hydrodynamic Resistance

[3] I.G. Currie, 2017, Fundamental Mechanics of Fluids, Fourth Edition, CRC Press

[4] Baldissera, Paolo, and Cristiana Delprete. "External and internal CFD analysis of a high-speed human powered vehicle." Int. J. Mech. Control 17 (2016): 27.

[5] Fegade, Vishal, Gajanan Jadhav, and M. Ramachandran. "Design, Modelling and Analysis of Tilted Human Powered Vehicle."
In IOP Conference Series: Materials Science and Engineering, vol. 377, no. 1, p. 012215. IOP Publishing, 2018.

[6] Bennett, Christopher, Nicholas Lawson, Falk Klinge, Julien Lefieux, and Cathal Moloney. "CFD and Wind Tunnel Analysis of the Drag on a Human-Powered Vehicle Designed for a Speed Record Attempt."
SAE International Journal of Vehicle Dynamics, Stability, and NVH 3, no. 10-03-02-0008 (2019).

[7] Alam, Firoz, Harun Chowdhury, Erika Guillaume, Jie Yang, and Gary Zimmer. "On-road and wind tunnel aerodynamic study of human powered vehicles."
 Procedia Engineering 60 (2013): 473-478.

[8] Baldissera, P., C. Delprete, and A. Gallo. "PulsaR design: CFD comparative study of speed-record Human Powered Vehicles." (2018).

[9] Collie, Scott. "Aerovelo Tops Human-Powered Speed Record with 89.59 mph Bullet Bike." *New Atlas*, 26 Sept. 2016, newatlas.com/aerovelo-eta-record-bike/45608/.